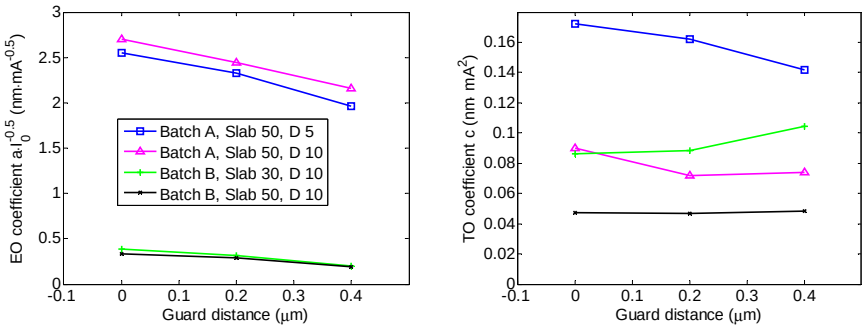

Fig. 4. Fitting results of the resonance wavelength model for devices with different fabrications, diameters (D), and slab heights: (a) EO effect (metric: $a/\sqrt{I_0}$); (b) TO effect (metric: c).

3.2. *Change of extinction ratio and quality factor*

When carriers are injected into a microring modulator, ER and $\mathbb{Q}$ change since the optical loss within the microring increases. The dependence of ER and $\mathbb{Q}$ on the intra-microring optical field loss coefficient α can be derived from Yariv's transmission relation in [23]:

$$T(\lambda) = 1 - \frac{(1-t^2)(1-e^{-2\alpha l})}{(1-te^{-\alpha l})^2 + (2t^{1/2}e^{-\alpha l/2}\sin(\pi n_{eff} l/\lambda))^2} \tag{7}$$

where t is the through-coupling coefficient that is related to the cross-coupling coefficient κ by $t^2+\kappa^2=1$; l is the microring circumference. The transmission spectrum around a resonance wavelength ($\lambda_r = n_{eff} l/m$) can be approximated by:

$$T(\Delta\lambda) = 1 - \frac{A}{1+(2\mathbb{Q}\cdot\Delta\lambda/\lambda_r)^2} \tag{8}$$

with

$$A = 1 - \left(\frac{t-e^{-\alpha l}}{1-te^{-\alpha l}}\right)^2, \quad \mathbb{Q} = m\pi\frac{t^{1/2}e^{-\alpha l/2}}{1-te^{-\alpha l}} \tag{9}$$

where A is related to ER by $ER = 1/(1-A)$. The loss coefficient α increases with the increase of the carrier concentration:

$$\alpha = \alpha_0 + n_a\Delta N = \alpha_0 + n_a\frac{Q_0}{2q\mathbb{V}}\left(\sqrt{1+\frac{4I\tau_0}{Q_0}}-1\right) \tag{10}$$

By incorporating Eq. (10) into Eq. (9), we can obtain the models for ER and $\mathbb{Q}$ as functions of the injected current I.

The effectiveness of the models is demonstrated by three devices with different coupling gaps on three coupling conditions, as shown in Fig. 5. In the over coupled case, the fitting parameter $t < \exp(-\alpha_0 l)$. As the injected current and thus optical loss increases, the $\exp(-\alpha l)$ decreases to be equal to t and then smaller than t. As a result, the ER (or A) first increases to reach infinity (or unity) from over coupled to critical coupled, and then decreases into the under coupled regime. Our model is consistent with the non-monotonic change of ER. In the over coupled case, the relatively large discrepancy between the model and the measurement may be due to the abrupt change of ER around the critical coupled condition. In the critical coupled (or under coupled) case, our model shows both good fitting results as well as reasonable fitting parameters with t equals to (or greater than) $\exp(-\alpha_0 l)$.

#235435 - $15.00 USD Received 26 Mar 2015; accepted 28 May 2015; published 4 Jun 2015

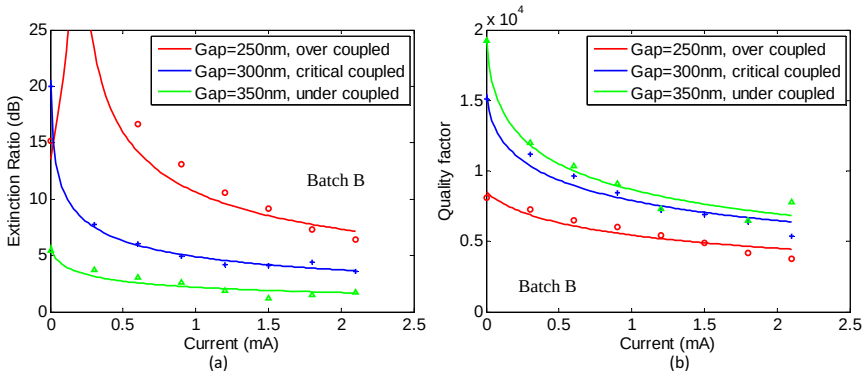

Fig. 5. Measured data (circles) and model fitting results (lines) for (a) extinction ratio and (b) quality factor of devices with different coupling gaps and coupling cases. The devices are from Batch B with a 5 μm diameter, a 0.4 μm guard distance, and a 50 nm slab height.

4. Electrical models

4.1. *DC model*

The governing equation describing the static I-V characteristics of the carrier-injection modulator is given by [21]:

$$I = I_S \exp\{q(V - IR - V_t)/(nkT)\} \tag{11}$$

where I_S is the reverse saturation current; R is the total series resistance including p/n doped region resistance, interconnect resistance and DC probe contact resistance during testing; n is the ideality factor. As illustrated in Fig. 6, the model shows that the devices with a diameter of 5 and 10 μm (denoted as D5 and D10) have similar V_t and n, while the resistance of D5 is almost twice of that of D10 because the microring circumference of D5 is half of that of D10.

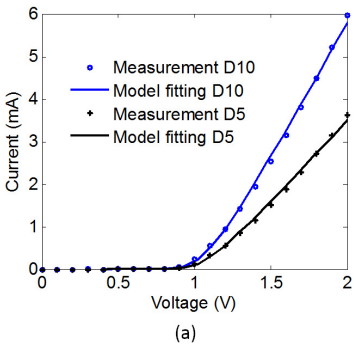

Ring diameter (μm)	V_t (V)	R (Ω)	I_S (nA)	n
10	0.427	147.0	2.196	1.905
5	0.403	240.3	1.000	1.956

(b)

Fig. 6. Measured and model fitted I-V curves of modulators with different diameters.

4.2. *Small-signal circuit model*

In order to better understand the high speed performance of the carrier-injection modulator, we develop a small-signal circuit model with physical origins as shown in Figs. 7(a) and 7(b). In the small-signal circuit, C_D and R_D respectively model the capacitance and resistance in the forward-biased p-i-n diode junction; C_{OX} denotes the capacitance through the cladding and

#235435 - $15.00 USD Received 26 Mar 2015; accepted 28 May 2015; published 4 Jun 2015

buried SiO_2 layers; R_{s1} and R_{s2} model the resistances of doped silicon; C_p represents the capacitance between the electrodes. The small-signal circuit parameters are extracted by measuring and curve-fitting the S11 test data. The Figs. 7(c) and 7(d) demonstrates the good curve-fitting results using the small-signal circuit model.

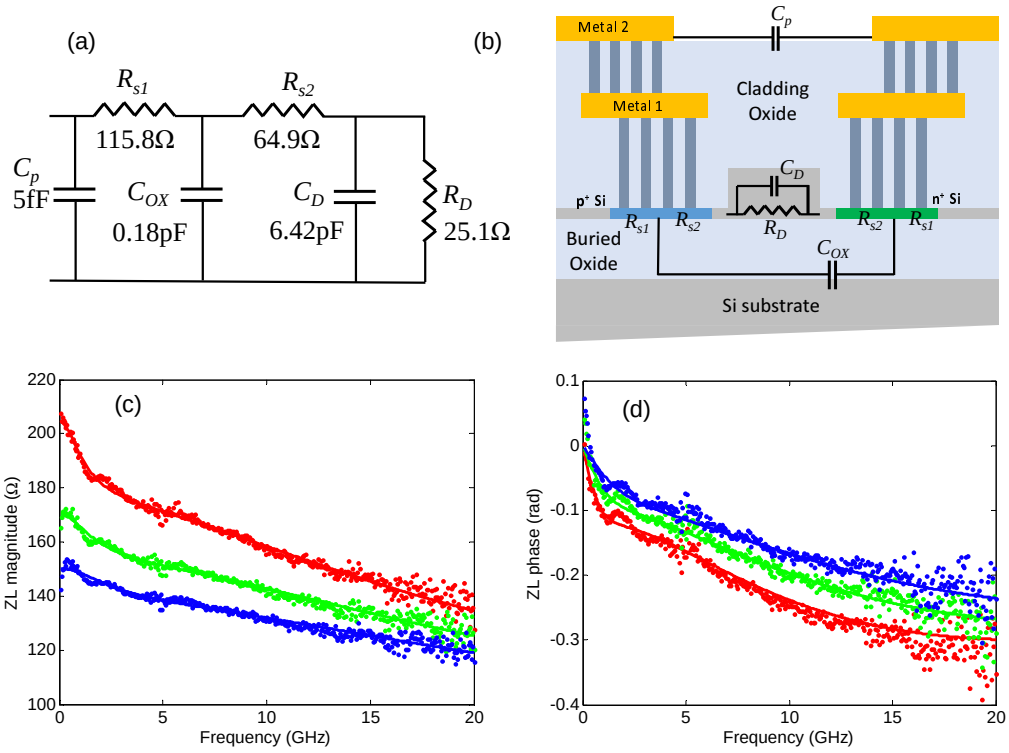

Fig. 7. (a) The small-signal circuit model with circuit values at 1mA bias points; (b) The cross-section of the microring waveguide; (c)(d) Curve-fitting of the measured load impedance Z_L of the modulator with a 10 μm diameter. (bias points: red 1 mA, green 2 mA, blue 3 mA)

Using the small-signal circuit model, we estimate the RC-limited 3dB frequencies for devices with different diameters and injection levels (Fig. 8). The equation for the RC-limited 3dB frequency is $1/(2\pi((R_{s1}+R_{s2})//R_D)C_D)$, based on the approximation that both C_p and C_{OX} are much smaller than C_D. From Fig. 8, one can see that the RC-limited device bandwidth increases with the increasing of the injection level. The Fig. 8 also demonstrates that the device with a 5μm diameter has a higher RC-limited bandwidth than that of 10 μm. It should be noted that though the carrier-injection modulator inherently has a low electrical bandwidth limit, the optical modulation speed can be greatly improved by using pre-emphasis schemes [2–5].

5. Model implementations in Verilog-A

The proposed DC and small-signal models have been implemented in Verilog-A. We use electrical voltage to mimic optical power, so that our Verilog-A models are compatible with common SPICE simulators. In the DC Verilog-A model, the optical output power is implemented as a function of the optical input power, the model parameters A, $\mathbb{Q}$ and λ_r, and the injected current. In the small-signal Verilog-A model, the small-signal circuit is represented by a RC network,

#235435 - $15.00 USD Received 26 Mar 2015; accepted 28 May 2015; published 4 Jun 2015

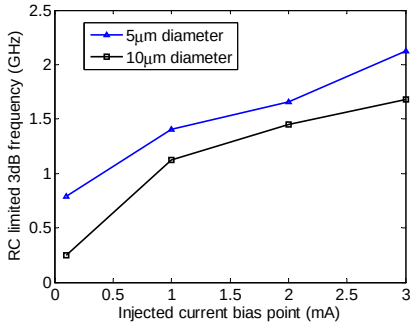

Fig. 8. The RC limited 3dB frequency predicted by the small-signal circuit model for devices with diameter of 5 μm and 10 μm at different bias points. The minimum bias point is 0.1 mA instead of 0 mA because the p-i-n junction needs a positive bias to be turned on for small-signal modulation. The guard distance of the microring modulator is 0.

where the current through R_D is the injected current I in the transmission spectrum model in the Section 3.

Our Verilog-A models can be used in the Synopsys HSPICE environment. Since it would be insightful to observe the device's characteristics with respect to applied voltages, we simulate the optical transmission versus applied voltage curves for a variety of operating wavelengths as shown in Fig. 9(a). One can see that as the operating wavelength deviates from the microring resonance wavelength, the optimal DC operating points (shown as black dots) varies. The maximum achievable extinction ratio also decreases as the operating wavelength deviates, because our DC models capture the dependence of ER on the injected current. Our small-signal model is used in the electro-optic AC simulations as shown in Fig. 9(b). The AC simulation results show that greater bias leads to a higher bandwidth, which agrees with the trend in Fig. 8.

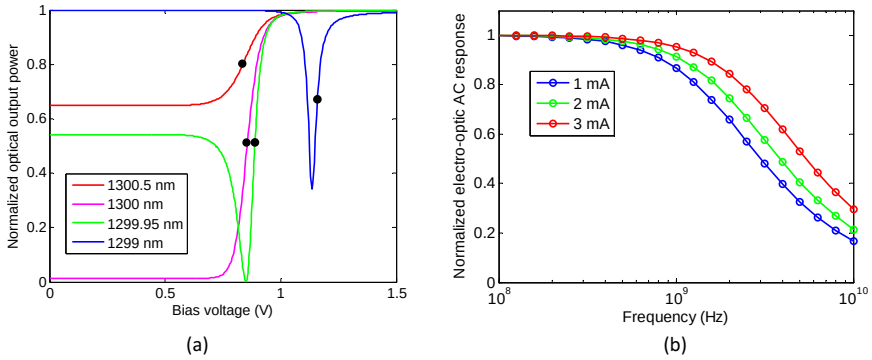

Fig. 9. (a) DC simulations of the modulator model for different operating wavelengths; the microring resonance wavelength at zero bias is 1300 nm; the black dots represent the optimal DC operating points for different wavelengths. (b) Electro-optic AC simulations of a microring modulator.

#235435 - $15.00 USD Received 26 Mar 2015; accepted 28 May 2015; published 4 Jun 2015

6. Conclusion

In this paper, we present theoretical DC models for carrier-injection microring modulators to characterize the resonance wavelength, quality factor, and extinction ratio with respect to the injected current. A small-signal circuit model is also proposed to characterize the high-speed performance of carrier-injection microring modulators. This set of models provides valuable physical insights to the device performance for a variety of designs and fabrication batches. We implement the proposed models in Verilog-A, which facilitates the SPICE-compatible co-simulation of electronic and photonic circuits.

Acknowledgments

The authors would like to thank Dr. Wayne Sorin and Dr. Tsung-Ching Huang from HP Labs, and Prof. John Bowers and Chong Zhang from UCSB for their helpful advises. R. Wu and K.-T. Cheng acknowledge the Semiconductor Research Corporation for the support.

#235435 - $15.00 USD Received 26 Mar 2015; accepted 28 May 2015; published 4 Jun 2015